ADVANCED FUNCTIONAL MATERIALS

Supporting Information

for *Adv. Funct. Mater.*, DOI 10.1002/adfm.202306399

Regulation Mechanism on A Bilayer Li_2O-Rich Interface between Lithium Metal and Garnet-Type Solid Electrolytes

Haoyang Jiang, Junqing Liu, Bin Tang, Zhendong Yang, Xinghui Liang, Xinyu Yu, Yirong Gao, Jinping Wei and Zhen Zhou**

Supporting Information

Regulation Mechanism on a Bilayer Li_2O-Rich Interface between Lithium Metal and Garnet-Type Solid Electrolytes

Haoyang Jiang, Junqing Liu, Bin Tang, Zhendong Yang, Xinghui Liang, Xinyu Yu, Yirong Gao, Jinping Wei, and Zhen Zhou**

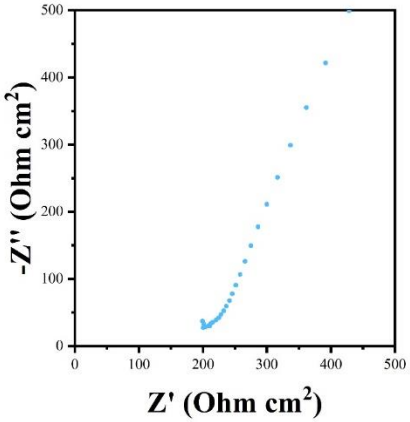


Figure S1. EIS measurement for LLZTO pellet. Au blocking electrodes were used and the measurement condition was room temperature.

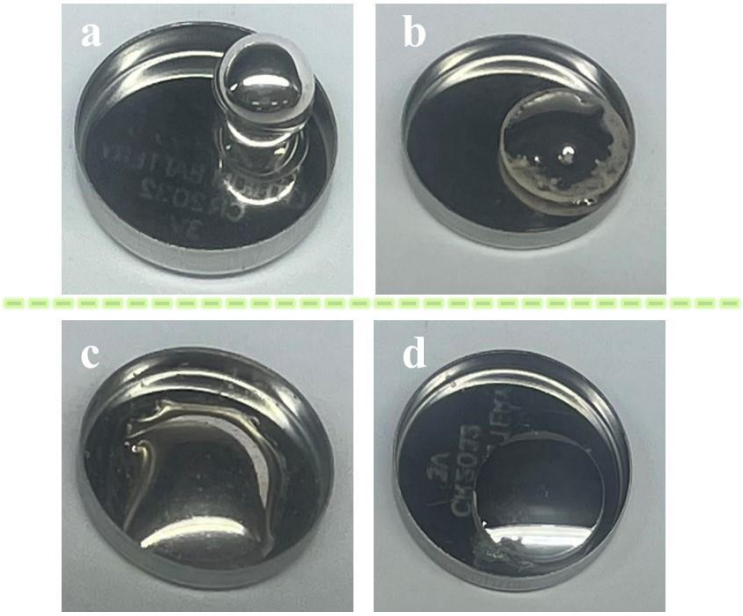


Figure S2. Digital photos of wettability evolution for molten Li after the addition of In_2O_3 at 240 °C. (a and b) Pure molten Li is shaped in sphere by surface energy and presents poor wettability on the LLZO surface. (c and d) Molten Li spread in the container and wet the pellet well, after In_2O_3 was added. Li still presents metal luster, with little white floating matter in the surface.

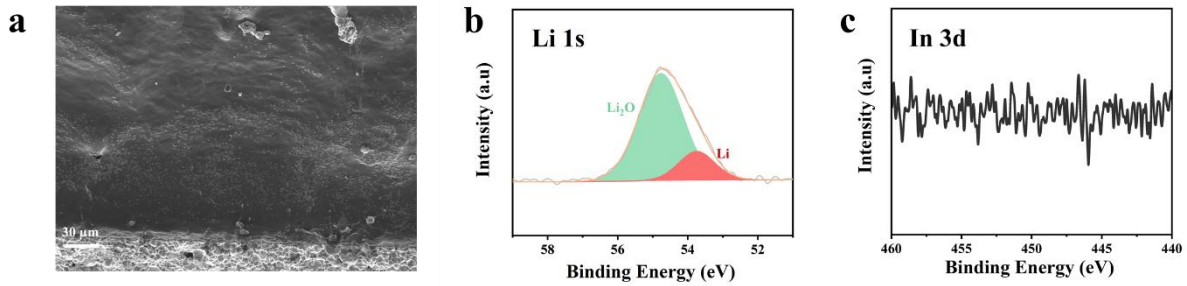


Figure S3. Characterizations of the anode Li after having reacted with In_2O_3. (a) SEM image of the Li anode. The small particles dissolved inside the anode bulk can be speculated to be Li-In alloys; however, they are hardly distinguished by EDS for the small size. (b and c) XPS analysis in the surface of Li anode, where the undetected In element can also evidence the above speculation.

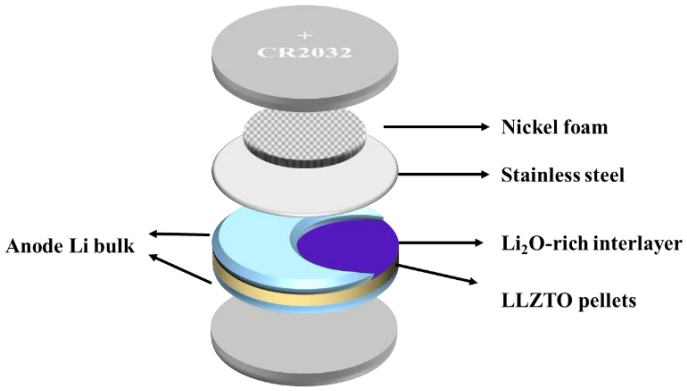


Figure S4. The construction of as-used Li/Li symmetric cells. The flatten nickel foam is used to immobilize the interior structure, inhibiting open-circuit due to poor contact.

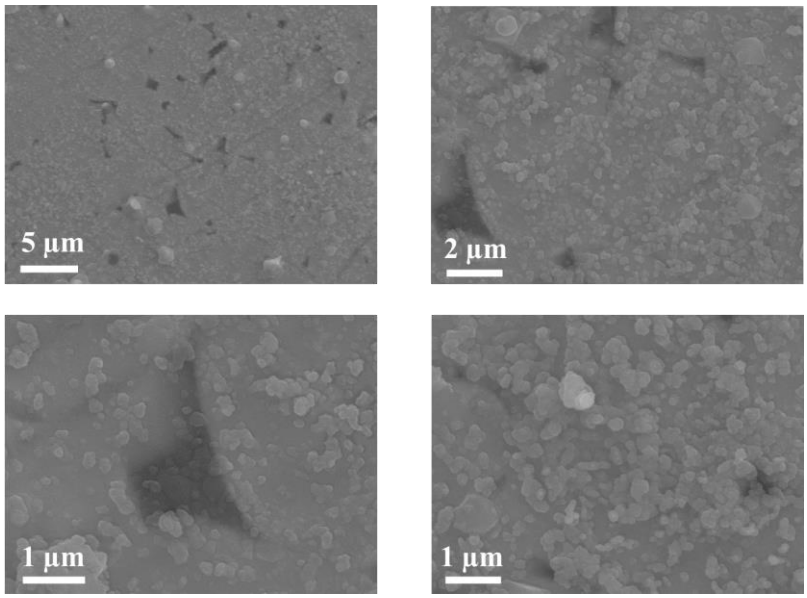


Figure S5. SEM images of the Li_2O-rich layer for Li-In_2O_3/LLZTO after peeling off the bulk Li. After peeling off the whole Li anode, the conformal Li_2O-rich layer is exposed. The scratches and defects indicate the rough LLZTO surface, which demonstrates that this Li_2O-rich layer is homogeneous even covering the defects.

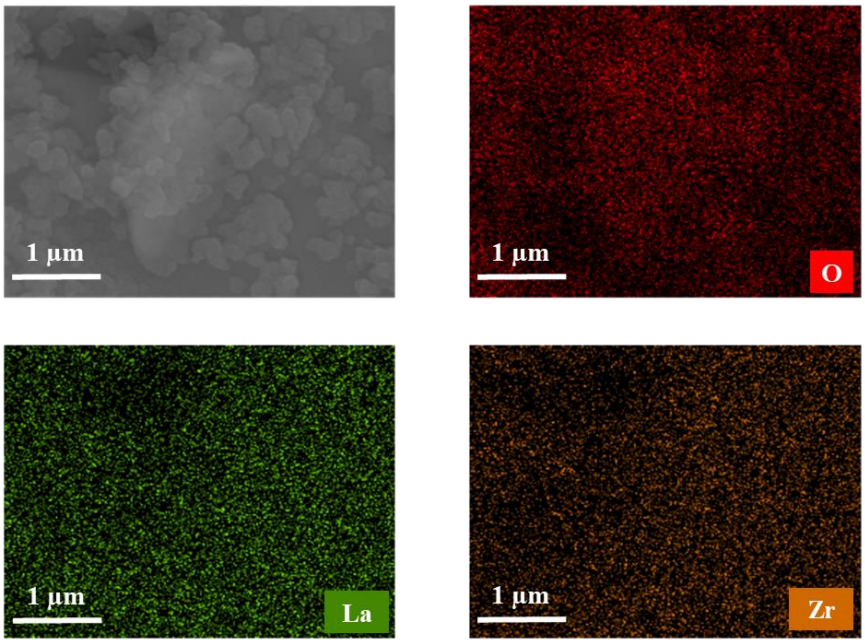


Figure S6. EDS images of the Li_2O-rich layer. SEM image of LLZTO surface after peeling off bulk Li. Corresponding EDS mapping of uniformly distributed La, Zr roots in LLZTO pellet, while, the clusters of red dots attribute to Li_2O clusters.

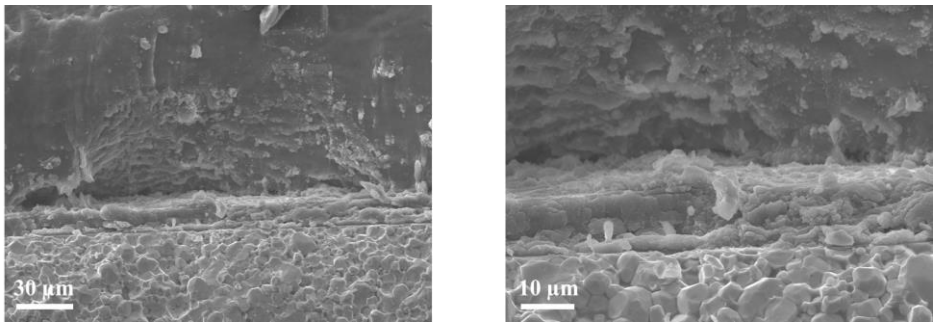


Figure S7. Cross-sectional images of the pulverized Li anode, related to Figure 3g. Cross-sectional image for Li-In_2O_3@LLZTO after cycling for 200 h at 30 °C.

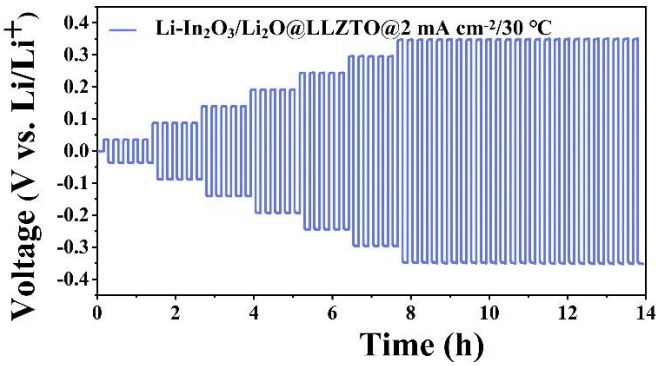


Figure S8. Galvanostatic cycling performance for Li-In_2O_3/Li_2O@LLZTO at 2 mA cm^{-2}, increasing from 0.2 mA cm^{-2} with the interval of 0.3 mA cm^{-2}.

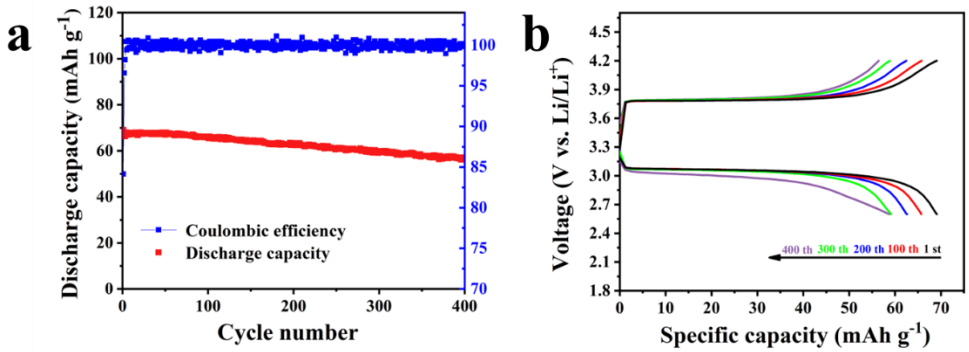


Figure S9. Long-time cycling stability of the full cells with Li-In_2O_3/Li_2O@LLZTO at 2 C and room temperature.

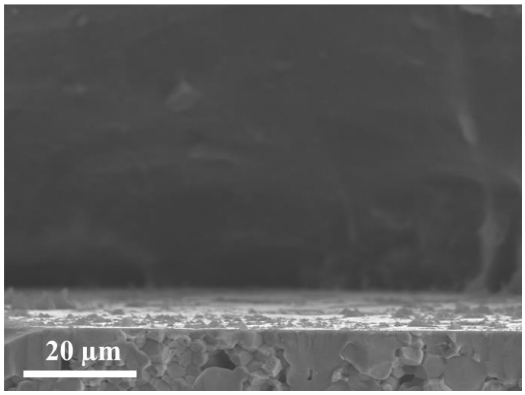


Figure S10. Amplified SEM image of the cross profile for pristine Li/LLZTO after stripping for 0.4 mAh cm^{-2}, related to Figure 5a. The discontinuous interlayer on the LLZTO surface is deficient for suppression of dendrites.

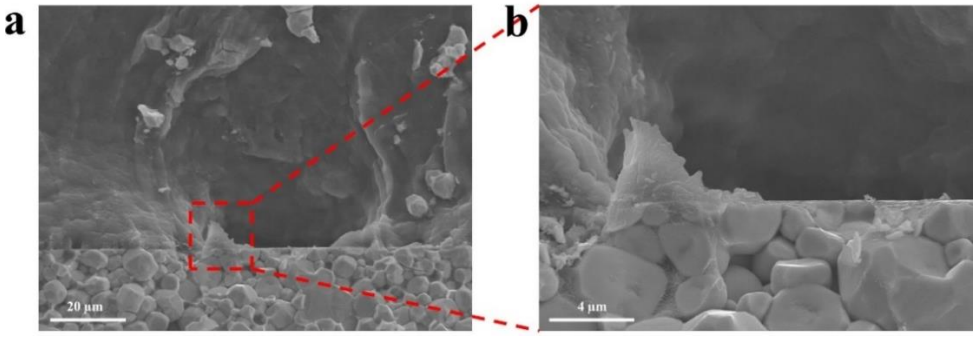


Figure S11. SEM images of cross profile for pristine Li/LLZTO after stripping for 0.4 mAh cm^{-2} and subsequent plating for 0.2 mAh cm^{-2}, related to Figure 5b. (a) The Li tends to deposit at the edge of voids, where "tip effect" provides huge driven energy. (b) Amplified view of (a) and there is obvious infiltrating Li in the grain boundaries under the deposited Li.

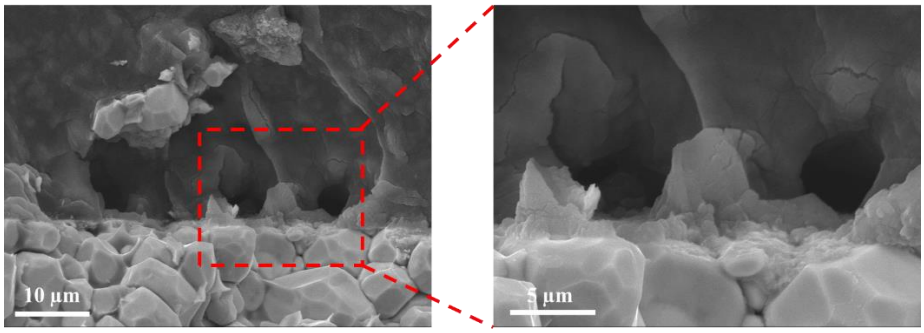


Figure S12. SEM images of cross profile for Li-In_2O_3/LLZTO after stripping for 0.4 mAh cm^{-2}, related to Figure 5c.

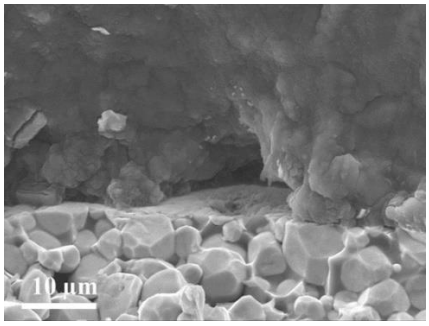


Figure S13. SEM image of cross profile for Li-In_2O_3/LLZTO after stripping for 0.4 mAh cm^{-2} and subsequent plating for 0.2 mAh cm^{-2}, related to Figure 5d.

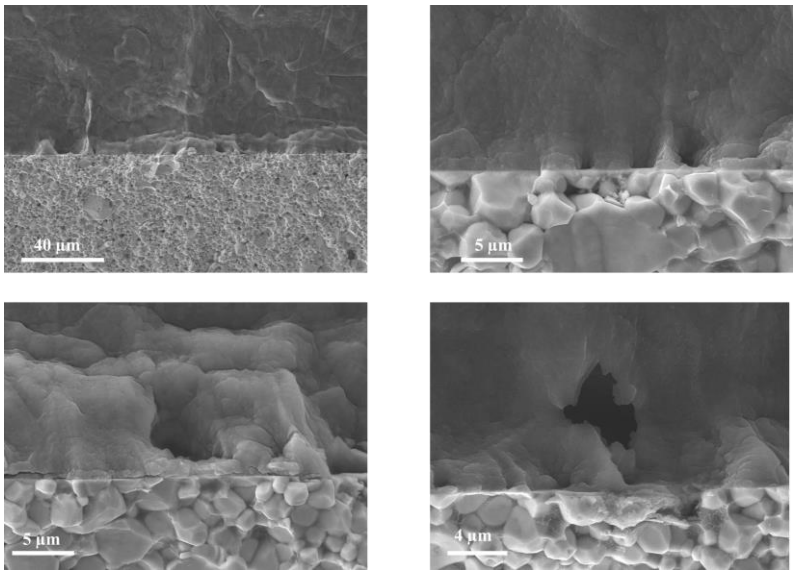


Figure S14. SEM images of cross profile for Li-In_2O_3/LLZTO after a complete cycle.

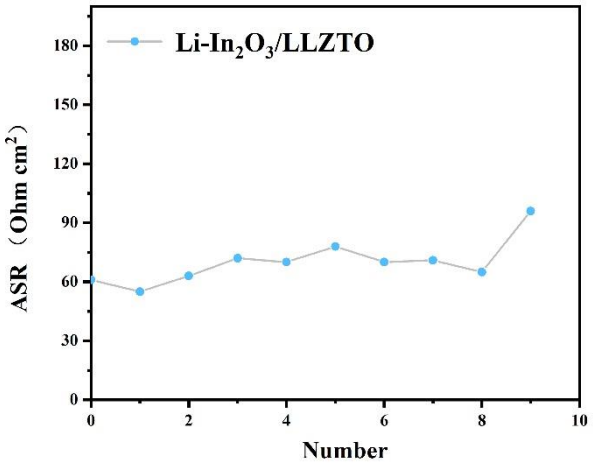


Figure S15. The ASR evolution at interface with relationship to depth of stripping at higher current density of 0.8 mA cm^{-2}. The sample interval is 2 mAh cm^{-2}.

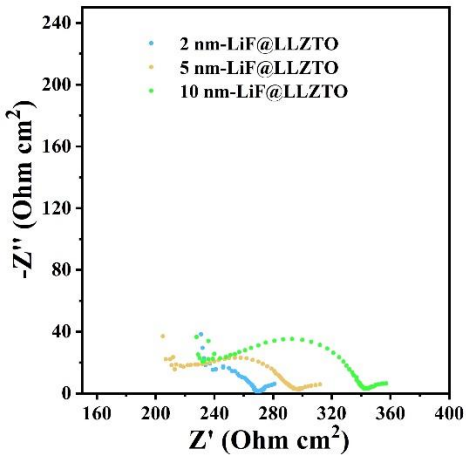


Figure S16. EIS measurements for LLZTO with 2, 5 and 10 nm LiF layer at 30 ℃.

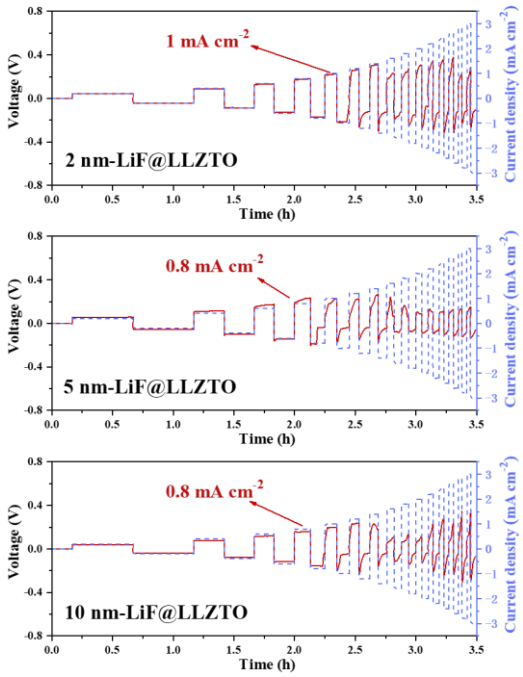


Figure S17. Critical current density measurement of LLZTO with 2, 5 and 10 nm LiF layer under stepwise increased current at 30 ℃.

Table S1. The electrochemical performance for stable cycling compared with previous reports.

Interfacial Strategy (thickness)	Method	Working Temperature (℃)	Interfacial ASR (Ω cm^{-2})	CCD (mA cm^{-2})	Current Density (mA cm^{-2})	Area Capacity (mAh cm^{-2})	Ref.
Ge (20 nm)	Electron beam evaporation (EBE)	RT	115	/	0.1	0.0083	[1]
Si (10 nm)	Plasma-enhanced chemical vapor deposition (PECVD).	RT	127	/	0.2	0.017	[2]
Al (20 nm)	Electron beam evaporation (EBE)	20	75	/	0.2	0.017	[3]
SnO_2 (12.3 nm)	ALD	RT	115	1.3	0.5	0.25	[4]
Porous Hard Carbon (10-20 nm)	Carbonizing phenolic resin and polyvinyl butyral layer	40	4.7	1.6	0.2	0.1	[5]
Li_3PO_4	ALD followed by annealing process	RT	1	2.2	1	0.5	[6]
$InCl_3$	Wet coating	RT	1	1.4	0.45	0.225	[7]
AlF_3	Li–Al alloy and LiF composite anode	RT	5	1.2	0.3	0.15	[8]
AlF_3 and AlN	Li–Al alloy and LiF/Li_3N composite anode	RT	2	1.1	0.5	0.25	[9]
SnF_2 (20 nm)	Thermal Evaporation	30	21	/	0.1	0.05	[10]
ITO (40 nm 90 wt% In_2O_3, 10 wt% SnO_2)	Magnetron sputtering	RT	32	1.05	0.2	0.2	[11]
In_2O_3 and Li_2O	Li_2O-rich interlayer and ALD Li_2O layer	30	22	2.4	2	0.25	This work

References

[1] W. Luo, Y. Gong, Y. Zhu, Y. Li, Y. Yao, Y. Zhang, K. Fu, G. Pastel, C.-F. Lin, Y. Mo, E. D. Wachsman, L. Hu, *Adv. Mater.* **2017**, 29, 1606042.

[2] W. Luo, Y. Gong, Y. Zhu, K. K. Fu, J. Dai, S. D. Lacey, C. Wang, B. Liu, X. Han, Y. Mo, E. D. Wachsman, L. Hu, *J. Am. Chem. Soc.* **2016**, 138, 12258.

[3] K. Fu, Y. Gong, B. Liu, Y. Zhu, S. Xu, Y. Yao, W. Luo, C. Wang, S. D. Lacey, J. Dai, Y. Chen, Y. Mo, E. Wachsman, L. Hu, *Sci. Adv.* **2017**, 3, e1601659.

[4] B. Tang, L. Gao, J. Liu, S.-H. Bo, Z. Xie, J. Wei, Z. Zhou, *J. Mater. Chem. A* **2020**, 8, 18087.

[5] L. Chen, J. Zhang, R. A. Tong, J. Zhang, H. Wang, G. Shao, C. A. Wang, *Small* **2022**, 18, 2106142.

[6] T. Deng, X. Ji, Y. Zhao, L. Cao, S. Li, S. Hwang, C. Luo, P. Wang, H. Jia, X. Fan, X. Lu, D. Su, X. Sun, C. Wang, J. G. Zhang, *Adv. Mater.* **2020**, 32, 2000030.

[7] J. Leng, H. Liang, H. Wang, Z. Xiao, S. Wang, Z. Zhang, Z. Tang, *Nano Energy* **2022**, 101, 107603.

[8] Z. Yang, M. Li, G. Lu, Y. Wang, J. Wei, X. Hu, Z. Li, P. Li, C. Xu, *Small* **2022**, 18, 2202911.

[9] J. Wei, Z. Yang, G. Lu, X. Hu, Z. Li, R. Wang, C. Xu, *Energy Storage Mater.* **2022**, 53, 204.

[10] B. Hu, W. Yu, B. Xu, X. Zhang, T. Liu, Y. Shen, Y. H. Lin, C. W. Nan, L. Li, *ACS Appl. Mater. Interfaces* **2019**, 11, 34939.

[11] J. Lou, G. Wang, Y. Xia, C. Liang, H. Huang, Y. Gan, X. Tao, J. Zhang, W. Zhang, *J. Power Sources* **2020**, 448, 227440.